Characterization of active site structure in CYP121: A cytochrome P450 essential for viability of *Mycobacterium tuberculosis* H37Rv

[1]Kirsty J. McLean, [2]Paul Carroll, [1]D. Geraint Lewis, [1]Adrian J. Dunford, [3]Harriet E. Seward,

[1]Rajasekhar Neeli, [4]Myles R. Cheesman, [5]Laurent Marsollier, [6]Philip Douglas, [6]W. Ewen Smith,

[7]Ida Rosenkrands, [8]Stewart T. Cole, [1]David Leys, [2]Tanya Parish, and [1]Andrew W. Munro

[1]Manchester Interdisciplinary Biocentre, Faculty of Life Sciences, University of Manchester, 131 Princess Street, Manchester M1 7DN, UK. [2]Centre for Infectious Disease, Institute for Cell and Molecular Science, Barts and the London, Blizard Building, London E1 2AT, UK. [3]Department of Biochemistry, University of Leicester, Henry Wellcome Building, Lancaster Road, Leicester LE1 9HN, UK. [4]School of Chemical Sciences and Pharmacy, University of East Anglia, Norwich NR4 7TJ, UK. [5]Unité de Génétique Moléculaire Bactérienne, Institut Pasteur, Paris, France. [6]Department of Pure and Applied Chemistry, University of Strathclyde, Glasgow G1 1XL, UK. [7]Department of Infectious Disease Immunology, Statens Serum Institut, Artillerivej 5, DK-2300 Copenhagen S, Denmark. [8]EPFL SV GHI UPCOL, AI 2151 (Bâtiment AI), Station 15, CH-1015, Lausanne, Switzerland.

Supplementary Data

Supplementary Experimental Procedures and Results

Generation of CYP121 mutants: Mutagenesis of *CYP121* was done using the Stratagene QuikChange® site-directed mutagenesis kit for mutants A233G, F338H, S237A and S279A. PCR cycling parameters were: an initial denaturation step of 95 ºC for 1 min followed by 15 cycles of 95 ºC (45 s), 62 ºC (1 min) and 68 ºC (7 min) for denaturation, annealing and extension, respectively. Standard protocols were followed for all reactions. R386L and P346L mutants were amplified from WT *CYP121* plasmid DNA using forward primers containing unique restriction sites close to the incorporated mutation site, and a reverse primer hybridizing to a region containing a unique restriction site. PCR parameters were: an initial denaturation step of 95 ºC for 1 min followed by 30 cycles of 95 ºC (30 s), 58 ºC (45 s) and 72 ºC (1.5 min), followed by a final elongation step of 72 ºC (10 min). After amplification, the mutant fragments were cloned into pre-digested plasmid with the appropriate WT fragment removed, as indicated in Table S1 below. Plasmid DNA was prepared by standard methods from resulting transformant colonies and mutants were screened by appropriate restriction enzyme digestion. Mutant clones were confirmed by DNA sequencing (MWG Biotech, Germany) using generic T7 and T7 terminator oligonucleotide primers, allowing verification of entire gene sequences. Primers sequences used for *CYP121* mutant gene generation are detailed in Table S1 below.

Table S1: Oligonucleotide primers used for mutagenesis of *M. tuberculosis CYP121*
Mutagenesis of *CYP121* was done as described in the *Experimental Procedures* section in the main text of the manuscript and as described further above. Codons for the mutated amino acids are highlighted and nucleotide changes introduced are shown in bold text.

CYP121 Mutant	Oligonucleotide Primer(s)	Comments
A233G	5'-cgtcactttcttcggtg**g**cggcgtcatctcaac-3'	Removes an existing NaeI site *c.f.* WT (Reverse primer complementary).
F338H	5'-cctcgcacctcgcc**cat**ggccgcggccaacac-3'	Unique NcoI site (underlined) created.
S237A	5'-gccggcgtcatc**g**caaccgg**t**agcttcctcacc-3'	Unique AgeI site (underlined) created.
S279A	5'-gctgcgga**t**taatctc**g**cc ttcgccgacg-3'	Additional AseI site (underlined) created.
P346L	Forward: 5'-ttcggccgcggccaacacttctgtc**tt**gga-3' reverse 5'-gacagcttatcatcgataagctttaatgcgg-3'	Removes existing PfoI site *c.f.* WT. SacII site (underlined) used for cloning with HindIII site (underlined) from reverse primer into pre-digested WT clone.
R386L	Forward: 5'-gaccaattggtctggcgcacccgattccaa**ct**acgc-3' Reverse: 5'-gacagcttatcatcgataagctttaatgcgg-3'	MfeI site (underlined) in forward primer used for cloning with HindIII site in reverse primer into pre-digested WT clone.

Crystallization and structural elucidation of CYP121 mutant enzymes: PDB codes, crystallization data and refinement statistics for the A233G, S237A, S279A, F338H, P346L and R386L mutants are presented in Table S2 below.

Table S2: Crystallographic data collection and final refinement statistics

CYP121 mutant	A223G	S237A	S279A	F338H	P346L	R386L
PDB code	3CXV	3CY0	3CY1	3CXX	3CXY	3CXZ
Resolution (Å)	20-1.70	20-1.90	20-1.75	20-1.90	20-1.45	20-1.08
Outer shell (Å)	1.75-1.7	1.95-1.90	1.80-1.75	1.95-1.90	1.49-1.45	1.1-1.08
Completeness (%)	99.7	99.8	100	98.5	100	99.9
Unique reflections	49363	36503	42788	35865	78019	174111
I/σI	11.2(3.1)	10.1(2.1)	9.3(2.2)	9.7(2.6)	13.5(2.3)	12.4(1.9)
R_{merge} (%)	5.6 (35.2)	6.9 (47.2)	7.2 (38.0)	8.2 (45.2)	5.7 (40.5)	8.7 (55.2)
R	16.6 (18.5)	20.4 (24.1)	18.6 (21.0)	17.6 (24.5)	15.4 (22.5)	14.7 (31.7)
R_{free}	19.0 (24.8)	23.3 (30.9)	21.1 (27.2)	21.8 (29.6)	18.6 (29.9)	16.8 (33.6)
Rmsd bond length (Å)	0.011	0.015	0.014	0.017	0.011	0.010
Rmsd bond angle (°)	1.356	1.493	1.477	1.595	1.391	1.411
Average B ($Å^2$)	9.7	19.2	21.4	21.2	16.6	9.2
Total of non-H atoms	3628	3335	3554	3623	3864	4079

Immunodetection of native CYP121 in Mtb: Antiserum 1426D used for identification of CYP121 was raised as described in the *Experimental Procedures* section of the main paper. A Western blot demonstrating immunodetection of CYP121 is shown below in Figure S1.

Figure S1: Western blot demonstrating detection of CYP121 produced in *Mycobacterium tuberculosis*

Western blot was done as described in the *Experimental Procedures* section of the main paper. Lane 1 shows lack of reactivity of the 1426D antiserum to a non-specific, purified Mtb P450 (CYP125, 50 ng); lane 2 shows strong reactivity with pure CYP121 (50 ng); lane 3 shows reactivity with total Mtb H37Rv cell lysate (10 µg); lane 4 shows negligible reactivity with short term Mtb culture filtrate (10 µg). Relative sizes of protein markers (kDa) are indicated to the left of the blot. A band of ~44 kDa is observed in both the pure CYP121 and cell lysate lanes, demonstrating clearly the production of CYP121 protein in Mtb H37Rv cells. The predicted molecular mass of CYP121 is 43.3 kDa.

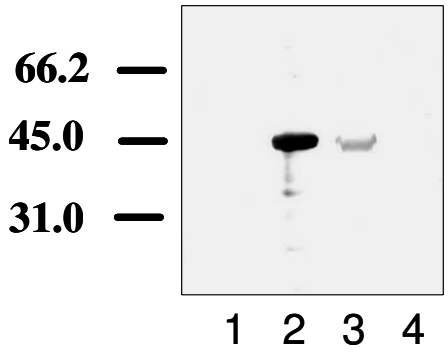

Ligand binding studies on CYP121 and active site mutants: Azole inhibitor titrations were done as described in *Experimental Procedures* in the main paper. Azole inhibitors were added in 0.1-0.5 µl aliquots using a Hamilton syringe for accuracy (Hamilton, Reno, NV). Total volume of ligand did not exceed 1 % of the overall volume. Spectra were recorded at each point in the titration. The spectrum for ligand-free P450 was then subtracted from each of the successive spectra collected during titrations to create a set of difference spectra. Peak and trough wavelengths were identified for each titration, and absorption values from the latter were subtracted from the former to generate an induced absorption difference at each point in the titration. All spectral data were corrected for dilution due to ligand additions, and no protein precipitation or development of turbidity was noted in the titrations. K_d values for azole binding to WT and mutant CYP121 proteins are presented in Table S3 below. A figure displaying structures of azole drug used is shown in Figure S2.

Table S3: K_d values for azole drug binding to *M. tuberculosis* CYP121 and mutants

The K_d values for azole antifungal drugs and for 2-phenylimidazole (2-PIM) and 4-phenylimidazole (4-PIM) were determined by optical titration as described in the *Experimental Procedures* section of the main manuscript. The K_d values for the tighter binding azole antifungal drugs were determined by fitting optical data to Equation 1 (defined in the main manuscript). The K_d values for the weaker binding phenylimidazole drugs were determined by data fitting to a standard hyperbolic function. The K_d values collected using Equation 1 are very sensitive to small changes in protein concentration used, and particularly in the very low K_d range (i.e. <1 µM). However, the K_d values for clotrimazole and econazole are clearly <0.2 µM in WT and mutants, and those for miconazole <0.5 µM. An exception is the F338H mutant, where the K_d for clotrimazole is clearly <0.5 µM, and that for miconazole is determined at 1.91 µM.

Inhibitor	Dissociation constant, K_d (µM)						
	WT	A233G	F338H	P346L	R386L	S237A	S279A
Clotrimazole	0.073 ± 0.008	0.092 ± 0.008	0.201 ± 0.041	0.121 ± 0.011	0.149 ± 0.016	0.069 ± 0.014	0.084 ± 0.009
Econazole	0.024 ± 0.006	0.065 ± 0.009	0.045 ± 0.010	0.049 ± 0.007	0.032 ± 0.004	0.043 ± 0.006	0.039 ± 0.005
Fluconazole	8.61 ± 0.21	14.6 ± 2.13	9.32 ± 1.10	16.1 ± 0.84	25.8 ± 1.41	11.8 ± 1.06	9.45 ± 0.087
Ketoconazole	3.44 ± 0.31	12.3 ± 0.09	5.17 ± 1.05	3.66 ± 0.26	5.95 ± 0.36	7.66 ± 1.02	4.08 ± 0. 37
Miconazole	0.136 ± 0.021	0.402 ± 0.05	1.91 ± 0.273	0.367 ± 0.053	0.259 ± 0.033	0.274 ± 0.041	0.213 ± 0.026
Voriconazole	16.3 ± 2.11	12.5 ± 2.32	25.8 ± 1.43	26.8 ± 3.29	18.4 ± 2.39	19.4 ± 3.15	23.1 ± 0.09
2-PIM	101.8 ± 9.33	124.8 ± 15.21	162.5 ± 17.9	147.3 ± 15.0	96.7 ± 10.8	86.4 ± 7.4	153.6 ± 17.4
4-PIM	32.3 ± 2.2	47.3 ± 3.7	13.5 ± 0.5	37.2 ± 1.9	44.9 ± 3.4	49.2 ± 3.3	40.3 ± 4.0

Figure S2: Structures of azole antifungal and phenylimidazole drugs used as CYP121 ligands in this study.

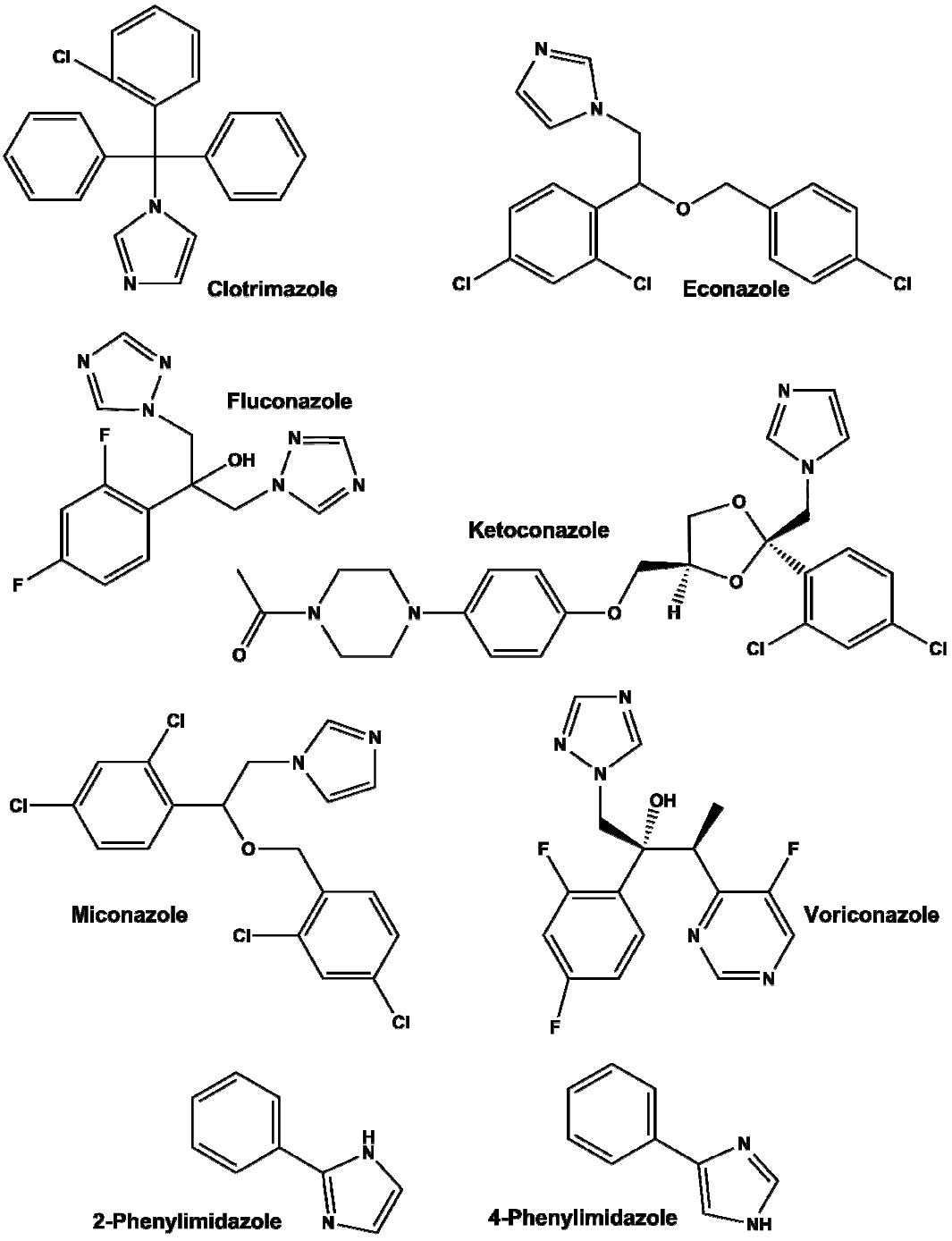

Determination of Mtb H37Rv MIC values: Azole susceptibility testing on *M. tuberculosis* H37Rv was done by radiometric measurements using the BACTEC 460 system (Becton Dickinson Diagnostic Systems, Sparks, MD), as described in *Experimental Procedures* in the main paper.

Studies of mycobacterial growth and anti-tuberculosis drug susceptibility are technically difficult and culture testing on solid media has many problems due to length of time required for visible growth (often many weeks of incubation) and differential results obtained. Focus is shifting to the use of liquid-based culture methods that are more rapid than conventional culture methods. The semi-automated radiometric mycobacterial detection BACTEC 460 system is most widely accepted as the reference standard for rapid identification and susceptibility testing of mycobacterial strains, and results are generally available within 10 days of incubation (reference S1). The basic principle of the BACTEC 460 TB system used is as follows. When mycobacteria grow in medium (typically Middlebrook 7H12) containing ^{14}C-labelled substrate (^{14}C-labelled palmitic acid is standard), they utilize the substrate and $^{14}CO_2$ is produced. The amount of $^{14}CO_2$ detected reflects the rate and amount of growth occurring in the vial, and is expressed in terms of the growth index (GI).

BACTEC drug susceptibility is determined by following a modified version of the conventional proportion method (e.g. reference S2). The critical proportion for resistance is taken as 1 % for all anti-tuberculosis drugs. This means that if 1 % or more of the test mycobacterial population is resistant, the culture is considered resistant for laboratory reporting purposes. Resistance is determined by comparing the rate of growth in the control vial and in vials containing the test drug. To determine the 1 % proportion of resistance, the bacterial inoculum used in the control vial is one-hundred fold less than that used for the drug-containing vial. The drug and control vials are tested daily after inoculation. The rate of increase in the GI, or the amount of change over that of the previous day, called the delta (Δ) GI, is compared between the control vial and the vials containing drugs. If the daily GI increase in the drug vial is equal to (or greater than) that in the control vial, the test organisms are considered resistant to the drug. For a susceptible population, the daily GI increase for the control would be higher than that of the drug vial. For example, if 1 % of the mycobacterial population is resistant to an anti-microbial agent, then 99 % of the organisms would be inhibited by the agent and only 1 % will grow in the drug vial. The growth rate in the drug-containing vial would then be similar to the growth rate in the control vial in which the original bacterial inoculum was only 1/100th of that in the drug-containing vial. The minimal inhibitory concentration (MIC) is defined as the lowest drug concentration that inhibits growth of more than 99 % of the bacteria.

Structural analysis of CYP121 enzymes: A representative image showing the electron density map superimposed onto the model of the CYP121 R386L mutant is shown in Figure S3 below. Following this, Figure S4 shows the relative degrees of distortion of the heme macrocycle (at pyrrole ring D) in the WT and P346L forms of CYP121.

Figure S3: Electron density map of heme in the CYP121 R386L structure
The image shows the heme group bound to the CYP121 R386L mutant and its associated heme ligands. The sigma-weighted $2F_oF_c$ density is contoured at 2 (in blue mesh) and 5 sigma (in red mesh) respectively.

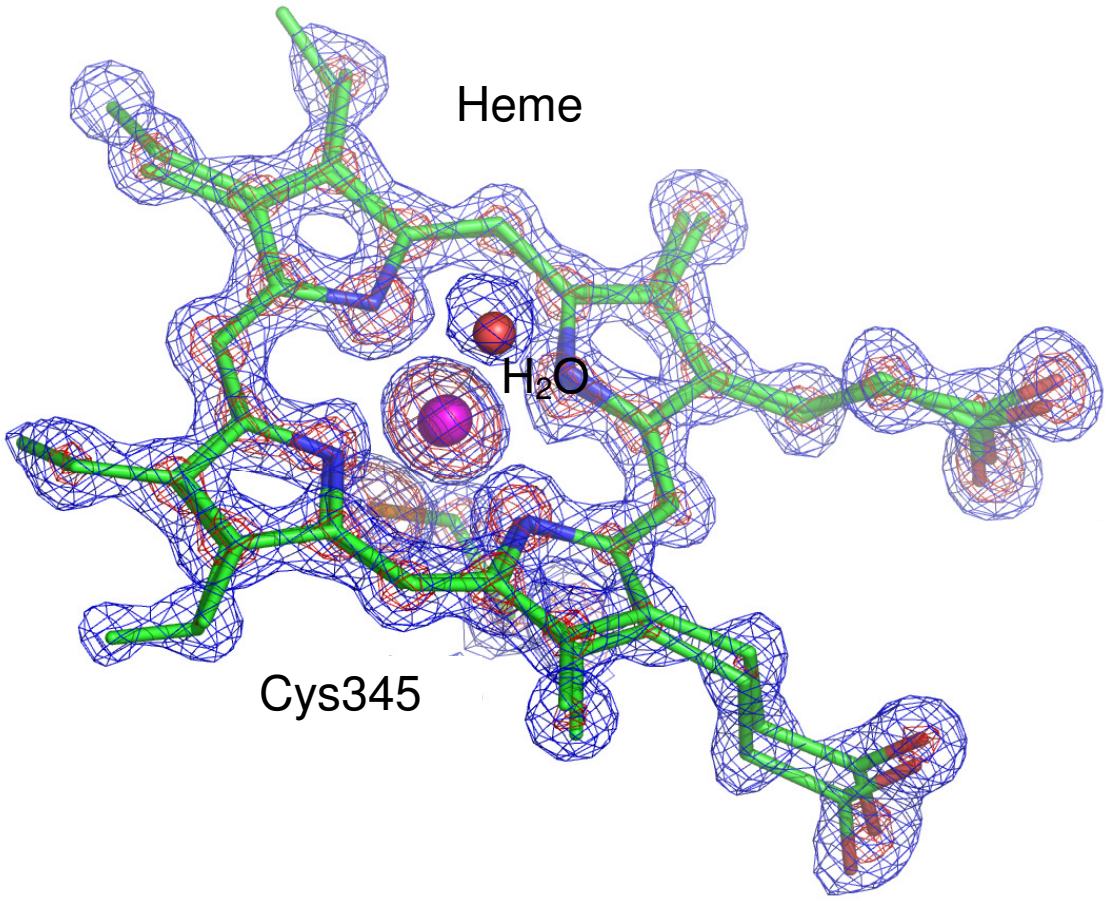

Figure S4: Overlay of heme groups in WT CYP121 and the P346L mutant
The image shows an overlay of the CYP121 heme group, its proximal ligand (Cys345) and the adjacent amino acid (Pro346 or Leu346) for WT CYP121 (PDB code 1N40; atom coloured sticks with green carbons) and for the P346L mutant (PDB code 3CXY; yellow carbon atoms). Black lines indicate the deviation of the pyrrole group D due to steric hindrance with the Pro346 (or Leu346) side chain. The P346L mutation gives rise to multiple conformations of the Leu346 side chain and multiple corresponding positions of the pyrrole group D.

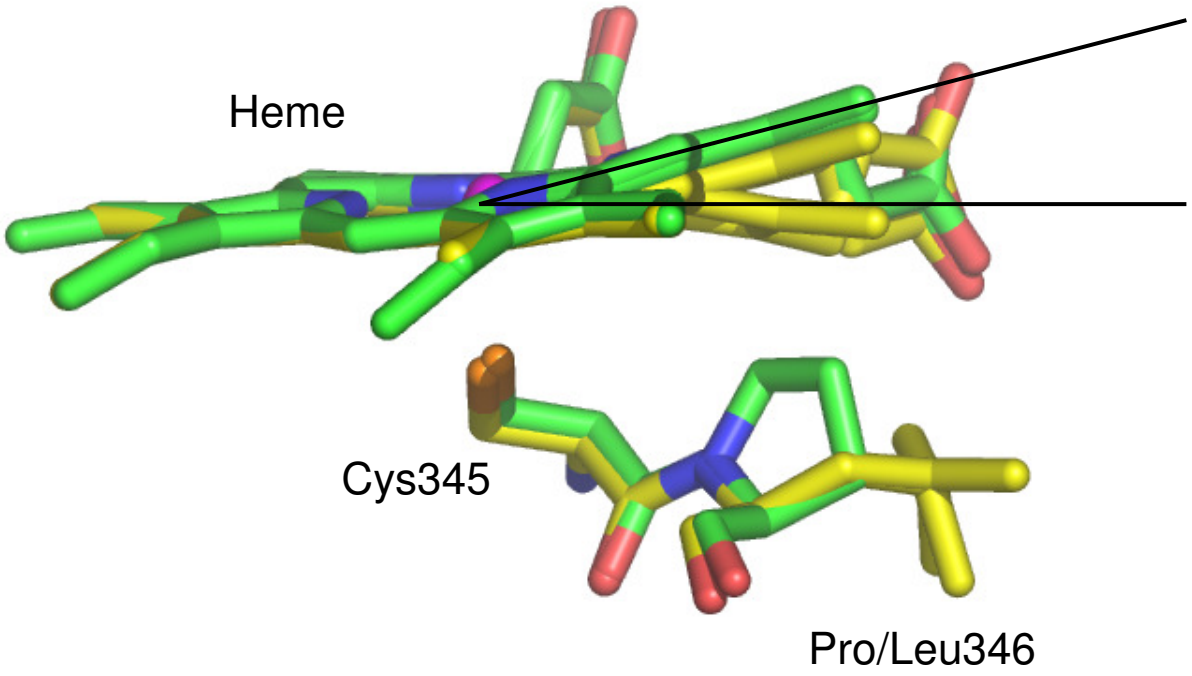

Determination of heme iron reduction potentials in CYP121 active site mutants: Redox potentials for the P450 heme iron were determined for each of the six CYP121 mutants according to established methods that we have used widely in previous studies of both WT CYP121 and other P450 enzymes (see references 22,27,33-35 in the main paper). Anaerobic spectroelectrochemical titrations were performed for the CYP121 enzymes (typically 5-15 μM in 100 mM potassium phosphate, pH 7.0). Enzymes were titrated with reductant (sodium dithionite) and oxidant (potassium ferricyanide) in presence of mediators (to expedite communicate between oxidant/reductant, enzyme and electrode) and to various states of reduction of the heme iron. The applied potential (measured *via* a calomel electrode immersed in the enzyme solution) and UV-visible absorption spectrum were recorded simultaneously. A fibre optic probe was immersed in the enzyme solution and linked to a Cary UV-50 spectrophotometer outside the glove box in order to record absorption spectra (typically 750-250 nm). Absorption values (in the Soret region and reflecting the maximal overall absorption change between the ferric and ferrous forms of the P450s) were plotted against the relevant applied potential and data were fitted using the Nernst equation (with Origin software), to determine the midpoint reduction

potential for the P450 heme iron in each case. Mediators used were phenazine methosulfate (PMS, 2 μM), 2-hydroxy-1,4-naphthoquinone (HNQ, 7 μM), methyl viologen (MV, 0.3 μM) and benzyl viologen (1 μM), to mediate in the range from 100 to -480 mV. Redox titrations were performed at 25 °C and usually completed in a period of 3-4 hours. Exemplary spectral data from the redox titration of the CYP121 P346L mutant are shown in Figure S5 below.

Figure S5: Spectroelectrochemical redox titration of CYP121 P346L mutant

Selected UV-visible absorption spectra from the spectroelectrochemical titration of the P346L mutant are shown. Redox titration was done as described in the *Experimental Procedures* section of the main manuscript and in *Supplementary data* descriptions above. The most intense spectrum (thick solid line) is that for the ferric enzyme (~12 μM), while the final spectrum (thin solid line) shows an extensively reduced enzyme. Intermediate spectra are shown as dotted lines. The absorption peak is at approximately 420 nm for the Soret band in the reduced form of the P346L mutant (compared to ~407 nm in the reduced R386L mutant, see Figure 5 in main paper) and there is also a feature at ~559 nm in the visible region for the reduced P346L enzyme. The development of these features is consistent with a slightly larger proportion of thiol-coordinated ferrous enzyme in the P346L mutant compared to the R386L mutant. Our recent studies demonstrated that (in the ferrous state) the CYP121 heme iron proximal ligand is in a reversible equilibrium between cysteine thiolate and thiol forms (see reference 57 in main manuscript). The redox potential determined from fitting P346L absorption change *versus* applied potential data to the Nernst equation was -458 ± 7 mV.

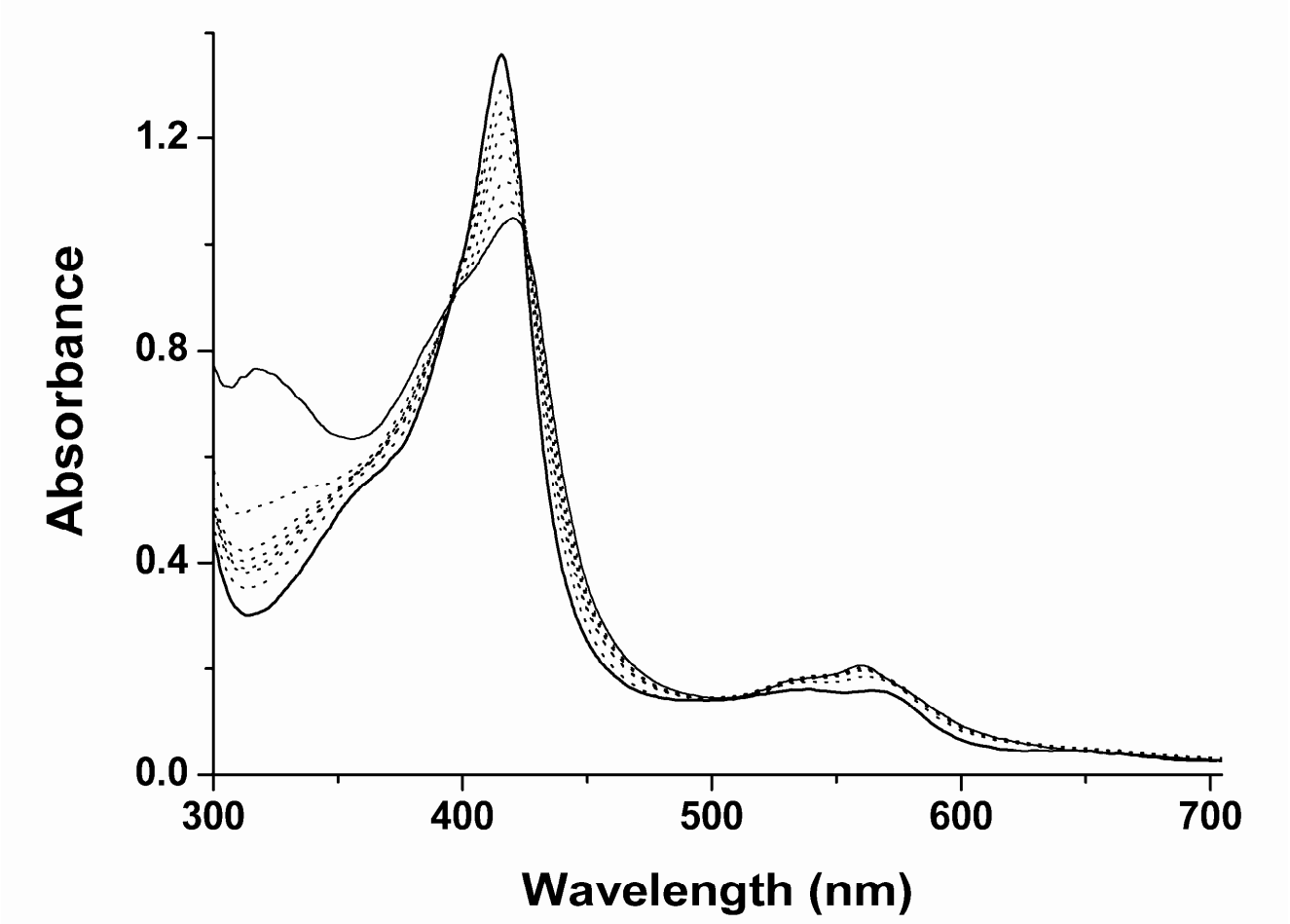

Resonance Raman analysis of CYP121 mutants: Major Resonance Raman (RR) features relating to heme iron oxidation, coordination and spin-state of CYP121 mutants (and their variations with WT CYP121) are discussed in the main paper. Other major differences between the WT and mutant CYP121 protein RR spectra include a downshift in frequency for the $\nu_{C=C}$ band in the heme proximal face mutants P346L and F338H, from 1623 ± 1 cm^{-1} (WT and other mutants) to 1619 cm^{-1} and 1615 cm^{-1}, respectively. This is a vinyl stretching vibration assigned to the in-plane conformer, with the out-of-plane mode obscured by the ν_{10} band. These data may indicate that the heme 2- and 4-vinyl groups lie more in the plane of the porphyrin for the P346L and F338H mutants than for the WT CYP121 (reference 50 in main paper). The ν_{13} band is in the so-called "fingerprint" (middle frequency, 1300-1000 cm^{-1}) region for specific heme-protein interactions, in which a number of bands originate from stretching vibrations of heme C_b-substituent bonds, with considerable influence from C_b-CH_3 vibrations (reference 49 in main paper). The ν_{13} band is downshifted for F338H (1218 cm^{-1}) compared to the other CYP121 enzymes (1224 cm^{-1}), likely reporting again on alteration in substituent group conformations for this mutant. There are also considerable changes in relative contributions of the two component species of the $=CH_2$ rock signal, with the lower frequency bands becoming more intense for P346L (1050 cm^{-1}) and for R386L (1056 cm^{-1}) by comparison with the higher frequency species (1090 cm^{-1}); whereas the reverse is the case for the other proteins. This again points to changes in the conformations of vinyl groups and alterations in conjugation of these substituents with the porphyrin ring system (reference 51 in main paper).

With respect to the fluconazole complexes of the various CYP121 proteins, there is decreased intensity of the ν_{37} band in WT and all mutants except R386L (where there is an apparent small increase in intensity). The ν_{37} vibration has E_u symmetry and previous studies have indicated that asymmetric conjugation of the vinyls can activate E_u modes, and thus distortion of vinyls away from the heme plane may occur in the fluconazole complex in WT and most CYP121 mutants (reference S3). The ν_{10} band that originates from a C_aC_m asymmetrical stretching mode is very prominent in the ligand-free R386L mutant, but becomes less well distinguished in the fluconazole complex as a result of the broadening of the $\nu_{C=C}$ vinyl stretching band. The ν_{10} band in WT and other mutants is seen as a shoulder in ligand-free and ligand-bound forms. The ν_{11} band is affected by electronic conjugation of the porphyrin and the vinyl groups, and is also sensitive to the nature of the axial ligands to the heme iron. It broadens and decreases in intensity in the fluconazole complexes of WT and the mutants (including S237A, where it is likely that contributions from the ν_{38} band obscure ν_{11}) (reference 53 in main paper).

The intensity of the ν_7 band of the heme skeleton increases in each of the CYP121 WT/mutant fluconazole complexes, and there are also shifts in both frequency and intensity for the δ_{vinyl} and δ_{prop} bending modes, again pointing to changes in conformation of substituent groups on the binding of fluconazole (reference S4, reference 51 in main paper).

Figure S6 below shows exemplary RR spectra for the A233G and R386L CYP121 mutants. This is followed by Tables S4 and S5, which show RR assignments for ligand-free WT and mutant CYP121 enzymes, and comparative data for ligand-free/fluconazole-bound CYP121 enzymes, respectively.

Figure S6: Resonance Raman analysis of A233G and R386L CYP121 mutants

Resonance Raman (RR) spectra are overlaid for the CYP121 A233G mutant (upper spectrum) and for the R386L mutant (lower spectrum). Major features are assigned according to standard nomenclature (reference 50 in main paper). The most intense feature is the ν_4 oxidation state marker band, which is located at 1373 cm^{-1} and is indicative of a ferric heme iron state in both proteins. A major difference observed is in the relative contributions of the 6-coordinate low-spin (6CHS) and 5-coordinate high-spin (5CHS) components of the spin-state marker band ν_3. The signals indicate an extensively low-spin species in the R386L enzyme and a mixed-spin species in A233G. Other features are discussed in the *Results and Discussion* section of the main paper and in *Supplementary data* above, and RR spectral assignments are presented in *Supplementary data* Tables S4 and S5 below.

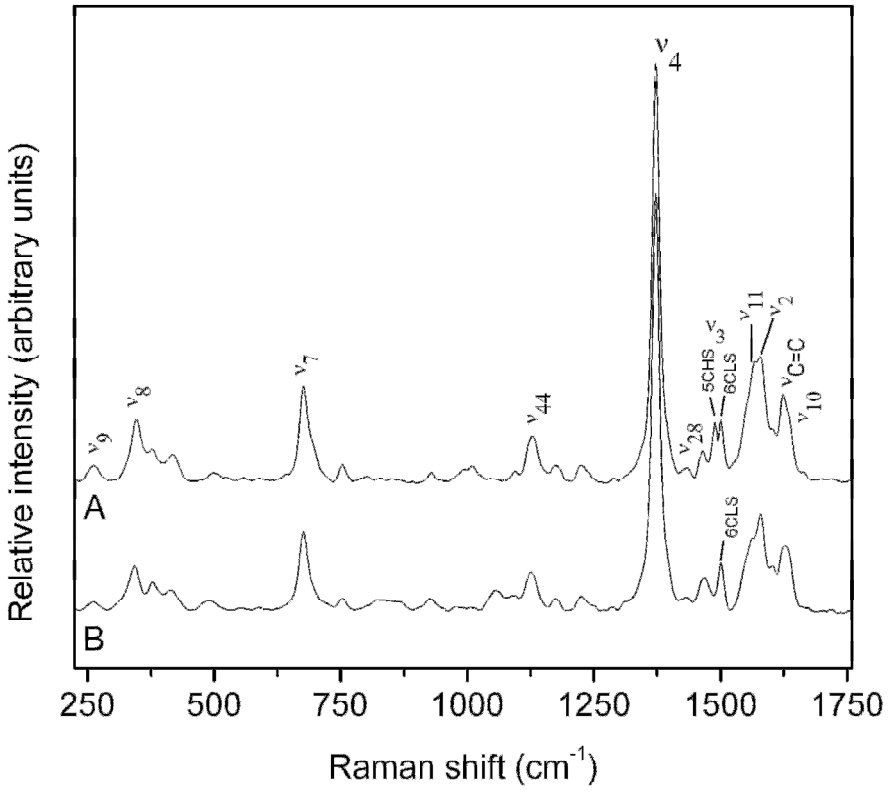

Table S4: Resonance Raman spectral assignments for ligand-free WT and mutant CYP121 enzymes

Resonance Raman data were collected using 406.7 nm radiation as described in the *Experimental Procedures* section of the main manuscript. Data were fitted using GRAMS software and the identified features are classified according to nomenclature described in reference 50 of the main manuscript. "Pyr. fold" indicates the feature associated with heme pyrrole folding vibrations.

Assignment	Band position (cm^{-1}) ligand-free CYP121						
	WT	**A233G**	**F338H**	**P346L**	**R386L**	**S237A**	**S279A**
ν_4	1372	1373	1372	1372	1373	1373	1373
ν_{10}	1634	1635	1632	1631	1633	1635	1633
$\nu_{C=C}$	1624	1624	1615	1619	1622	1624	1623
ν_{37}	1601	1603	1602	1604	1601	1601	1603
ν_2	1580	1579	1579	1580	1578	1579	1580
ν_{11}	1557	1568	1557	1563	1564	1556	1564
ν_{38}	1525	1524	1522	1522	1532	1525	1525
ν_3	1501 (6CLS) 1487 (minor)	1501 1489 (40%)	1500 1487 (minor)	1500 1486 (minor)	1500	1500 1488 (45%)	1502 1486 (<1%)
ν_{28}	1469	1466	1464	1467	1466	1463	1466
δ_s (=CH_2)	1431	1434	1433	1433	1430	1431	1436
ν_{13}	1224	1224	1218	1224	1224	1224	1224
ν_{30}	1173	1173	1169	1176	1173	1173	1176
ν_{44}	1130	1129	1122	1125	1117	1130	1133
$\nu_6 + \nu_8$	1125	1119	1115	-	1110	1120	1127
=CH_2rock	1090 1049 (minor)	1094 1051 (minor)	1092 1050 (minor)	1090 1050 (major)	1090 1056 (major)	1091 1053 (minor)	1094 1054
γ (CH=)	1013	1009	997	1013	1010	1007	1011
$\nu_7 + \nu_9$	929	928	924	925	924	930	931
ν_{16}	752	754	750	753	752	752	752
ν_7	677	676	673	678	676	676	677
ν_{49}	549	551	554	553	549	560	558
Pyr. fold	494	500	498	492	482	504	507
δ vinyl	418	418	412	411	415	418	415
δ propyl	387	384	381	391	387	390	389
$2\nu_{35}$	378	378	375	378	378	375	378
ν_8	347	347	345	343	347	347	347
ν_9	262	261	288	263	261	261	261

Table S5: Comparison of Resonance Raman spectral assignments for fluconazole-bound and ligand-free forms of WT and mutant CYP121 enzymes

Resonance Raman data were collected using 406.7 nm radiation as described in the *Experimental Procedures* section of the main manuscript. Final fluconazole (fluc) concentration was 100 μM in all cases. Data were fitted using GRAMS software and the identified features are classified according to the nomenclature described in reference 50 of the main manuscript. Data are shown for major vibrational features and to emphasise those features for which some variations are seen between ligand-free and fluconazole-bound form of the enzymes. Relative intensities of the 6-coordinate low-spin (6CLS, at 1501 ± 1 cm^{-1}) and high-spin (at 1488 ± 2 cm^{-1}) components of the ν_3 spin-state marker band are indicated. Intensity values are reported relative to the value for the ν_4 band in wild-type CYP121. In the case of the ν_{10}, ν_{11}, δ_{vinyl} and δ_{prop} bands, the presence of the relevant feature as a shoulder or broad shoulder on another band is indicated where appropriate. In the case of the ν_{10} feature for the R386L mutant and the ν_{11} feature for the S237A mutant, the term "↑peak" indicates that a distinct band is either formed (for ν_{11}, S237A) or is lost to a shoulder on another feature (for ν_{10}, R386L) on the binding of fluconazole. For the ν_3 features, the approximate proportions of the high-spin (HS) species are estimated relative to the low-spin (LS) species. For selected wild-type and mutant CYP121 enzymes, the relative intensity of the lower frequency component of the $=CH_2$ rock feature (compared to the higher frequency component) is indicated by "major" or "minor" for the former component.

Enzyme	Raman shift (cm^{-1}) *(Relative Intensity)*												
	ν_4	ν_{10}	$\nu_{C=C}$	ν_{37}	ν_2	ν_{11}	ν_3	ν_{13}	$=CH_2$ rock	ν_7	δ_{vinyl}	δ_{prop}	ν_8
WT	1372	1634 *(1520)*	1624 *(3650)*	1601 *(1845)*	1580 *(2072)*	1557 *(2163)*	1501 *(2431)* 1487 *(540)*	1224 *(735)*	1090 *(2227)* 1049 *(1856)* minor	677 *(2784)*	418 *(244)*	387 *(327)*	347 *(1130)*
+ fluc	1372	1634 *(1956)*	1623 *(2430)*	1602 *(1188)*	1579 *(3467)*	1565 *(1137)* broad shoulder	1501 *(1539)*	1224 *(548)*	1089 *(1001)* 1046 *(901)* minor	677 *(5417)*	420 *(848)*	391 *(1233)*	347 *(2295)*
A233G	1373	1635 *(2276)*	1624 *(3002)*	1603 *(1843)*	1579 *(4362)*	1568 *(4145)*	1501 *(1862)* 1489 *(1724)* (45% HS)	1224 *(562)*	1094 *(333)* 1051 *(70)*	676 *(3369)*	418 *(935)*	384 *(1107)*	347 *(2180)*
+ fluc	1373	1635 *(1547)*	1623 *(2120)*	1601 *(1279)*	1580 *(3181)*	1569 *(2697)* broad shoulder	1501 *(1725)* 1488 *(312)*	1223 *(1341)*	1093 *(998)* 1051 *(740)*	677 *(5068)*	421 *(932)*	389 *(1093)*	347 *(2594)*
F338H	1372	1632 *(1859)*	1615 *(3713)*	1602 *(2516)*	1579 *(1894)*	1557 *(4515)*	1500 *(1535)* 1486 *(760)* (< 5% HS)	1218 *(475)*	1092 *(1175)* 1050 *(943)*	673 *(2896)*	412 *(862)*	381 *(935)*	345 *(1830)*
+ fluc	1370	1632 *(1579)*	1618 *(2422)*	1600 *(2061)*	1576 *(2901)*	1560 *(2540)* broad shoulder	1500 *(1648)*	1220 *(223)*	1092 *(1178)* 1050 *(1083)*	673 *(3678)*	417 *(819)*	387 *(998)* broad shoulder	345 *(1829)*
P346L	1372	1631 *(1870)*	1619 *(2089)*	1604 *(1575)*	1580 *(3422)*	1563 *(2537)*	1500 *(1734)* 1487 *(524)* (<1% HS)	1224 *(490)*	1090 *(519)* 1050 *(707)* major	678 *(2813)*	411 *(696)*	391 *(974)*	343 *(1574)*
+ fluc	1372	1629 *(1438)*	1622 *(1555)*	1604 *(931)*	1582 *(2036)*	1563 *(1274)* broad shoulder	1500 *(1789)*	1226 *(569)*	1090 *(1632)* 1050 *(1695)* major	677 *(5865)*	414 *(760)*	396 *(1055)*	345 *(1682)*
R386L	1373	1633 *(1726)* ↑ peak	1622 *(1936)*	1601 *(1058)*	1578 *(2620)*	1564 *(2060)*	1501 *(1529)*	1224 *(599)*	1090 *(3055)* 1056 *(1520)*	676 *(3943)*	415 *(1698)*	387 *(1042)*	347 *(2205)*
+ fluc	1374	1633 *(1743)* shoulder	1623 *(2093)*	1602 *(1150)*	1580 *(1925)*	1555 *(1105)* broad shoulder	1501 *(1673)*	1224 *(719)*	1090 *(3508)* 1056 *(1020)*	677*(5965)*	418 *(1932)* broad shoulder	389 *(1410)*	347 *(2124)*
S237A	1373	1635 *(1227)*	1624 *(1721)*	1603 *(1777)*	1579 *(2450)*	1556 *(1518)*	1500 *(847)* 1488 *(864)* (45% HS)	1224 *(360)*	1091 *(354)* 1053 *(202)*	676 *(1688)*	418 *(474)*	390 *(645)*	347 *(1151)*
+ fluc	1373	1633 *(2396)*	1623 *(3564)*	1603 *(1641)*	1578 *(3064)*	1549 *(2466)* ↑ peak	1500 *(2641)*	1226 *(1047)*	1091 *(705)* 1053 *(471)*	678 *(7403)*	419 *(118)*	387 *(248)*	349 *(1380)*
S279A	1373	1633 *(1982)*	1623 *(2466)*	1601 *(1473)*	1580 *(3682)*	1568 *(2677)*	1502 *(1775)* 1486 *(592)* (<1% HS)	1224 *(562)*	1094 *(896)* 1054 *(586)*	677 *(3394)*	415 *(940)*	389 *(1749)*	347 *(2333)*
+ fluc	1373	1635 *(1853)*	1622 *(2418)*	1603 *(1393)*	1580 *(3588)*	1560 *(2370)* broad shoulder	1502 *(1537)*	1224 *(493)*	1095 *(541)* 1054 *(373)*	677 *(4828)*	418 *(699)*	386 *(833)*	347 *(1961)*

Table S6: EPR g-values for wild-type and mutant forms of CYP121 proteins
EPR data were collected as described in *Experimental Procedures* in the main paper. Data confirm typical cysteinate coordination of ferric heme iron in each of the CYP121 P450s.

CYP121 protein	g-values		
	g_z	g_y	g_x
WT	2.47	2.25	1.91
A233G	2.45,2.51	2.26	1.92,1.89
F338H	2.48	2.25	1.91
P346L	2.49	2.26	1.90
R386L	2.44	2.25	1.92
S237A	2.45,2.44	2.26	1.92
S279A	2.47	2.25	1.92

Figure S7: EPR spectra for wild-type and mutant forms of CYP121 proteins
EPR data were collected as described in *Experimental Procedures* in the main paper. The g-values in Table S6 were determined from spectral data presented in this figure.

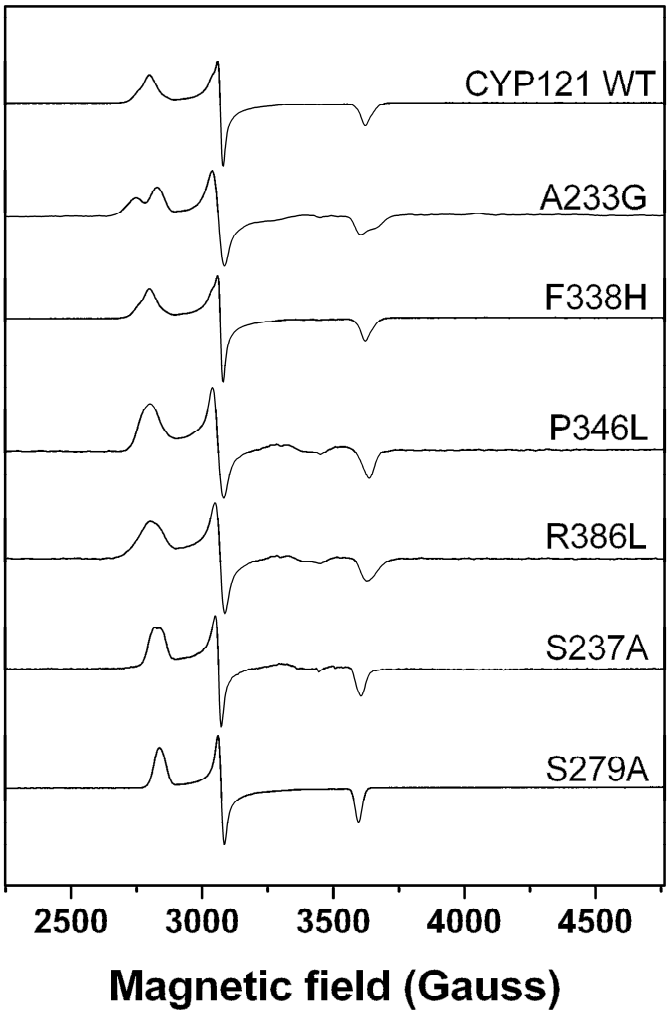

Supplementary references

S1) Roberts, G.D., Goodman, N.L., Heifets, L., Larsh, H.W., Lindner, T.H., McClatchy, J.K., McGinnis, M.R., Siddiqi, S.H., and Wright, P. (1983) *J. Clin. Microbiol*. **18**, 689-696.
S2) Garrigó, M., Aragón, L.M., Alcaide, F., Borrell, S., Cardeñosa, E., Galán, J.J., Gonzalez-Martín, J., Martin-Casabona, N., Moreno, C., Salvado, M., and Coll, P. (2007) *J. Clin. Microbiol*. **45**, 1766-1770.
S3) Choi, S., Spiro, T.G., Langry, K.C., Smith, K.M., Budd, D.L., and Lamar, G.N. (1982) *J. Am. Chem. Soc*. **118**, 4345-4351.
S4) Matsuura, K., Yoshioka, S., Tosha, T., Hori, H., Ishimori, K., Kitagawa, T., Morishima, I., Kagawa, N., and Waterman, M.R. (2005) *J. Biol. Chem*. **280**, 9088-9096.